symmetry

MDPI

Article

Study on the Crystal Structure of Coal Kaolinite and Non-Coal Kaolinite: Insights from Experiments and DFT Simulations

Peng Xi [1,*], Ruixin Ma [1,*] and Wenli Liu [2]

[1] Department of Environmental Engineering, North China Institute of Science and Technology, Beijing 101601, China

[2] School of Chemical and Environmental engineering, China University of Mining and Technology (Beijing), Beijing 100083, China; lwl@cumtb.edu.cn

* Correspondence: pengxi@ncist.edu.cn (P.X.); maruixin@ncist.edu.cn (R.M.); Tel.: +86-136-4125-7510 (P.X.)

Received: 18 June 2020; Accepted: 3 July 2020; Published: 6 July 2020

Abstract: Coal is often coated by kaolinite in flotation, leading to a decrease in the quality of clean coal. The structure of the mineral determines its properties and flotation behavior. Therefore, to remove the kaolinite from coal efficiently, the difference in mineralogical characteristics between non-coal and coal kaolinite were analyzed using advanced instruments. The experiment results showed that, due to the substitution of the C atom for Si atom, the interplanar spacing of the kaolinite (001) surface became small with C-O-C, Al-O-C, and C-O-Si covalent bonds formed instead of Al-O-Si and Si-O-Si bond. Based on this, the models of monolayer and bilayer coal kaolinite (001) surfaces were built and the structure difference was compared through DFT calculation. The calculation results showed that the silicon atom of the kaolinite Si-O-(001) surface was easier to be doped by carbon atoms with external energy as the interplanar spacing of the kaolinite (001) surface decreased with the increase in doped carbon atoms (7.15440 Å→7.11859 Å→7.10902 Å→7.10105 Å). The structural difference between non-coal kaolinite and coal kaolinite were compared from the view of the experiment and quantum chemistry, which provides an important theory for subsequent research on the properties of coal kaolinite and its further processing and utilization.

Keywords: crystal structure; coal kaolinite; density functional theory (DFT); symmetry structure

1. Introduction

In the process of coal slime flotation, a large number of fine-grained coal clay minerals are mixed into the clean coal, whose composition is mostly kaolinite [1]. This limits the efficiency of flotation and reduces the quality of clean coal [2]. The surface properties of coal kaolinite are the key factors to determine its surface floatability [3] and the surface properties depend on the surface crystal structure [4]. The previous study found that the coal pyrite surface was substituted [5] and covered [6] by carbon atoms so that the structure and properties of coal pyrite were different from the non-coal pyrite [7]. Meanwhile, the formed sulfur after optimization enhanced the hydrophobicity of coal pyrite [8]. Therefore, it is very important to accurately obtain the crystal structure information of kaolinite for understanding the physical and chemical properties and flotation characteristics of kaolinite [9]. Coal kaolinite has formed special crystal structures in the long-term coal forming environment due to the lattice defect and surrounding rock symbiosis and has further significantly exhibited different surface properties from the non-coal kaolinite. Because the kaolinite and other clay minerals exist as microcrystalline or cryptocrystalline, it is difficult to measure the microstructure of coal kaolinite thoroughly and comprehensively by experimental means. Many scholars have studied

the crystal structure of kaolinite by calculation. However, there are few reports on the calculation and experimental study of coal kaolinite.

The first principles on the basis of DFT were carried out to study the crystal structure of the mineral surface and its structural parameters. Hong [10] constructed the kaolinite unit cell model. Zhang [11] constructed an interlayer cluster model of kaolinite. Zhao [12] found that Fe and Cr atoms can easily be doped into the kaolinite lattice structure, while Ca, Mn and Be atoms can be doped into the kaolinite lattice at a higher temperature. Han's calculation [13] showed that there is a positive charge on the Al-(001) surface of kaolinite. On the contrary, there is a negative charge on the Si-(001) surface. Tunega, D. [14] calculated the bond strength and length of the pkaolinite crystal cell based on the first principles. Zhang [15] found that the interlayer charge of soft kaolinite is higher than hard kaolinite, and the crystallinity of the former is higher.

In the paper, two types of kaolinite—non-coal kaolinite and coal kaolinite—from the China ore district are studied and tested by SEM, XRD, FTIR and XPS. The differences in morphological characteristics, phase composition, molecular structure and elemental form are compared. The single-layer and double-layer crystal structure models of coal kaolinite are put forward, which provide an important theoretical basis for the subsequent study of the properties of the coal kaolinite surface and its further processing and utilization.

2. Materials and Methods

2.1. Samples

The kaolinite and coal kaolinite of China, typically mined from different areas, were selected as the research object, as shown in Table 1. K-1 represented the powder non-coal kaolinite from Zhangjiakou in the Hebei province. CK-2 represented the lump coal kaolinite from Datong in the Shanxi province. CK-3 represented the lump coal kaolinite from Huairen in the Shanxi province. CK-4 represented the powder coal kaolinite from Huaibei in the Anhui province. X-ray fluorescence spectrometry (XRF) was carried out using the ARL ADVANT'X IntelliPower^{TM} 3600 of Thermo Fisher Scientific. Whether the non-coal kaolinite or the coal kaolinite, the contents of the SiO_2 and Al_2O_3 were close to the theoretical chemical composition of pure kaolinite. The selected samples were very pure, which met the requirements of pure minerals for the test.

Table 1. Experimental samples and their composition

Compound	K-1	CK-2	CK-3	CK-4
SiO_2/%	54.76	54.10	54.05	52.17
Al_2O_3/%	43.16	44.60	44.41	45.32
TiO_2/%	0.69	0.43	0.46	0.68
Fe_2O_3/%	0.56	0.18	0.21	0.58
P_2O_5/%	0.01	0.01	0.02	0.40
CaO/%	0.03	0.09	0.37	0.26
Na_2O/%	0.09	0.02	0.06	0.19
MgO/%	0.16	0.04	0.09	0.13

2.2. Experimental Equipment and Methods

The four samples were characterized using SEM, XRD, FTIR and XPS. The appearances of the samples were observed by the Hitachi SU8020 Scanning electron microscope, whose magnification was 30–800,000×. XRD were carried out with the Bruker D8 ADVANCE X-ray diffractometer and the samples were ground under a 200 mesh. The tube voltage and the tube current were 40 kV and 40 mA, respectively. A Cu target and a wavelength of 1.5406 Å was selected. The scanning scope is generally 10–90° and adjusted according to the sample difference. The scanning speed was set up to 0.06 s/step. The step interval was 0.02°/step. FTIR spectra were attained with a Thermo Fisher Scientific Nicolet-IS5 spectrometer. The sample and KBr (1:100), which were mixed and pressed into pellets, were scanned

at the range of 4000–400 cm^{-1}. All samples were dried at 105 °C for 4 h before measurement. The XPS experiment was carried out with a Thermo Scientific Escalab 250Xi X-ray photoelectron spectroscope, made by Thermo Fisher Scientific. The Al target X-ray source with monochromator was used for testing in an ultra-vacuum environment. The vacuum degree of the analysis chamber was greater than 1×10^{-9} mbar. The value of the pass energy, energy step and spot size was 20 eV, 0.05 eV and 900 um, respectively.

2.3. Computational Methods and Models

2.3.1. Computational Method

The optimized single-layer model of the kaolinite (001) surface was attained from Han [16,17] with the CASTEP of Materials Studio software [18]. The generalized gradient approximation (GGA), developed by Perdew–Burke–Ernzerhof (PBE), was selected as the exchange–correlation function. The interactions between valence electrons and the ionic core were represented using the ultra-soft pseudopotentials [19]. The cut-off energy was 400 eV. All the calculations were run until the energies were converged to within 2.0×10^{-6} eV/atom in each self-consistency cycle and the forces on all ions were converged to within 0.05 eV/Å. The threshold values for the other convergence criteria were 0.002 Å for maximum displacement, 0.1GPa for maximum stress, 2.0×10^{-5} eV/atom for energy and DFT-D correction was adopted [20,21]. The atomic positions were optimized by the Broyden–Fletcher–Goldfarb–Shanno (BFGS) algorithm [22]. In the geometric optimization process of bulk kaolinite, all atoms and unit cell parameters were relaxed so that the optimized primitive unit cell were close to the experimental values. We optimized the carbon atom, silicon atom, oxygen atom and water molecule by the $20 \times 20 \times 20$ cubic cell whose Brillouin zone sampling was restricted to k-point, and the other parameters were consistent with the primitive unit cell optimization, reported above.

2.3.2. Surface Model

The model of the kaolinite (001) surface was cleaved from the kaolinite unit cell, which was exposed with a hydroxylated and a siloxane on each side of the surface. We used the periodic supercell ($2 \times 1 \times 1$), which had a vacuum thickness of 20 Å [23]. The slab was comprised of "H-O-Al-O-Si-O", six atomic "sublayers", which were optimized with three "sublayers" fixed. Two sides of the kaolinite (001) surface model were studied—Al-O-(001) surface and Si-O-(001) surface—as shown in Figure 1a. The double-layer model of the kaolinite surface constructed in the paper is based on the single-layer model, as shown in Figure 1b. The double-layer model of kaolinite is optimized to get the optimal exchange–correlation function and cutoff energy, as shown in Table 2. The rationality of the double-layer was determined according to the error ratio, which is calculated as:

$$E_r = \frac{|d_e - d_c|}{d_e} \quad (1)$$

where E_r was the error rate, d_e was the experimental value of the interplanar spacing, which was 7.1453 in the paper, consistent with the other experimental values of 7.19 [24], 7.15 [25,26], 7.17 [27]. d_c was the calculated value of the interplanar spacing. The smaller the E_r , the more rational the double-layer structure of kaolinite.

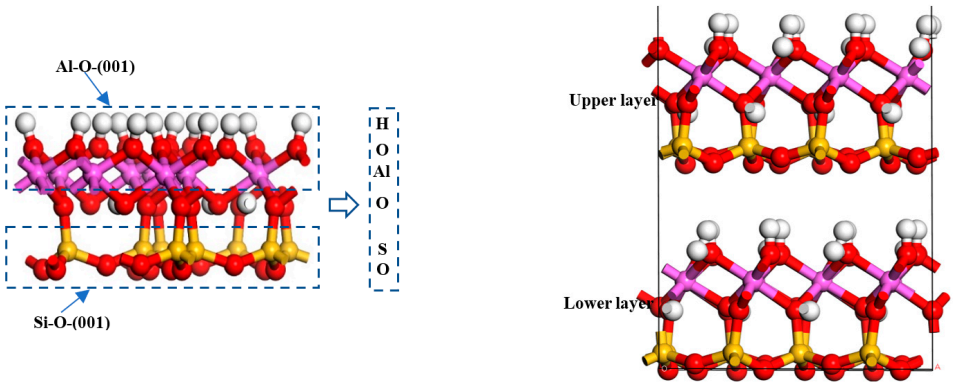

Figure 1. The structure model of the kaolinite (001) surface: (**a**) single-layer; (**b**) double-layer.

Table 2. Optimized results of the kaolinite double-layer model.

Exchange–Correlation Function	Cutoff Energy/eV	Interplanar Spacing	Error Ratio/%
GGA-PBE	400	7.0503	1.45
GGA-RPBE	400	7.1544	0.00
GGA-PW91	400	7.4109	3.59
GGA-WC	400	7.4250	3.78
GGA-PBESOL	400	7.3457	2.67
LDA-CA-PZ	400	6.8943	3.63
GGA-RPBE	300	7.2197	0.91
GGA-RPBE	350	7.1974	0.60
GGA-RPBE	450	7.1224	0.45
GGA-RPBE	500	7.1074	0.65
Experimental value		7.1543	

From Table 2, we can see that the interplanar spacing of the kaolinite double-layer (001) surface in different exchange–correlation functions and cut-off energies were obtained and the error ratio was calculated. The error ratio of the interplanar spacing on the condition GGA-RPBE and 400 eV is minimal (0.00), which explained that the calculated interplanar spacing was closest to the experimental value. The double-layer model of the kaolinite (001) surface was the most reasonable. The model of subsequent coal kaolinite (001) surface was constructed based on the optimized kaolinite (001) surface.

2.3.3. The Impurity Substitution Energy

The model of the kaolinite surface containing defects was optimized by impurity substitution energy [28]. Its value represented the difficulty of the substitution, defined as:

$$\Delta E = E_{total/C} + E_X - E_{total/perfect} - E_C \quad (2)$$

where ΔE is the impurity substitution energy in this paper, meaning the energy needed for substitution, and $E_{total/C}$ is the energy of the kaolinite surface substituted by the carbon atom. $E_{total/perfect}$ is the energy of a perfect surface. E_X and E_C are the energies of the single Si atom (or O atom) and C atom. If the ΔE was positive, the substitution can occur with the external energy. The larger the value, the more the needed energy, which means it is more difficult to replace an atom.

3. Results and Discussion

3.1. Mineralogical Characteristics

3.1.1. SEM

The surface morphologies of all kaolinite samples were analyzed by field emission scanning electron microscopy, and the results are shown in Figure 2. The non-coal kaolinite has a structure of stacked layers, some of which are rhombic and hexagonal and some of which are irregular due to fragmentation, and the surface is smooth and clean without impurities. The coal kaolinite (CK-2, CK-3, CK-4) is also structured with stacked layers, some of which have rough surfaces and impurities clearly attached to them. It is preliminarily concluded that the surface of coal kaolinite may contain carbon impurities that have not been fully dissociated and it may contain lattice defects which lead to the incomplete crystal structure.

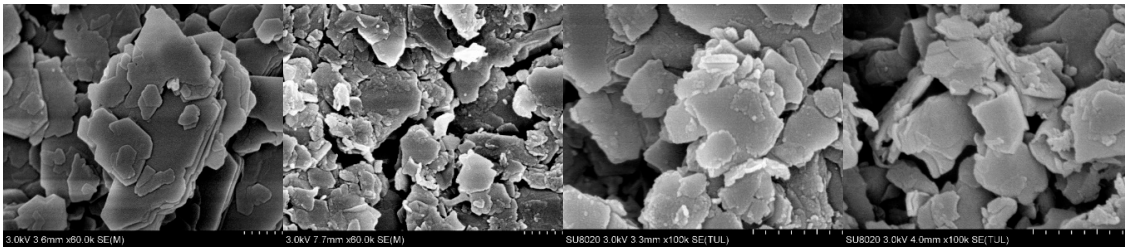

(**a**) (**b**) (**c**) (**d**)

Figure 2. The surface morphology of all kaolinite samples. (**a**) K-1; (**b**) CK-2; (**c**) CK-3; (**d**) CK-4.

3.1.2. XRD

Atoms with a similar radius and charge or net polarity substitute the atoms of crystal, which is called lattice substitution. It may be either stoichiometric or nonstoichiometric. XRD is an effective technique to analyze the lattice defect state of the mineral surface. On the basis of the above surface morphology by SEM, the XRD test was carried out to analyze the characteristic peak offsets or the new peak presences of the samples. The phase composition can be determined and the interplanar spacing calculated. Furthermore, the lattice impurity can be determined [29]. The XRD results in Figure 3a show that:

(a) Although non-coal and coal kaolinite belong to different types, the diffraction peak position and intensity of the XRD powder diffraction pattern are basically the same, and the peak position and intensity are consistent with the crystal diffraction data of the PDF standard card, as shown in Figure 3a. Among them, the intensity of the diffraction peak (001) is the strongest, the peak (002) is the second, and the content of kaolinite (001) is the highest, which is the most easily dissociated (001) in the process of fragmentation.

(b) Further comparative analysis shows that the diffraction peak position of non-coal kaolinite (001), shown in Figure 4b, is consistent with that of standard card kaolinite (001) (2θ = 12.362°). However, the peak position (2θ = 12.382°) of coal kaolinite from Datong (CK-2) is shifted to the right, and the peak position (2θ = 12.405°) of coal kaolinite from Huairen (CK-3) is shifted to the right with a larger angle. The peak position (2θ = 12.368°) of coal kaolinite from Huaibei (CK-4) is also shifted to the right. The characteristic peak offsets of the coal kaolinite may be attributed to isomorphism, including silicon atom doping by the carbon atom, aluminum atom, iron atom or other atoms.

$$2d_{HKL}sin\theta = n\lambda \quad (3)$$

where the d_{HKL} was the interplanar spacing, θ was the angle between the incident X-ray and the corresponding crystal plane, λ was the wavelength of the X-ray and n was the diffraction series.

According to the Bragg's law (2) and the wavelength of the Cu target (λ = 1.5406Å), the interplanar spacing of the samples (001) are calculated as follows:

$$d_{K-1} = \frac{1.5406}{2 \times \sin 6.181} = 7.1543\ A; \quad d_{CK-2} = \frac{1.5406}{2 \times \sin 6.191} = 7.1430\ A;$$

$$d_{CK-3} = \frac{1.5406}{2 \times \sin 6.202} = 7.1304\ A; \quad d_{CK-4} = \frac{1.5406}{2 \times \sin 6.184} = 7.1508\ A;$$

It was found that, due to the long-term coal forming environment, the carbon atom with smaller atomic radius (0.077 nm) in the coal may replace the silicon atom with larger atomic radius (0.117 nm) in the coal kaolinite (CK-2, CK-3, CK-4), which leads to the contraction of the crystal (001) surfaces and a decrease in the interplanar spacing. On the X-ray diffraction peak, it moves towards a large angle.

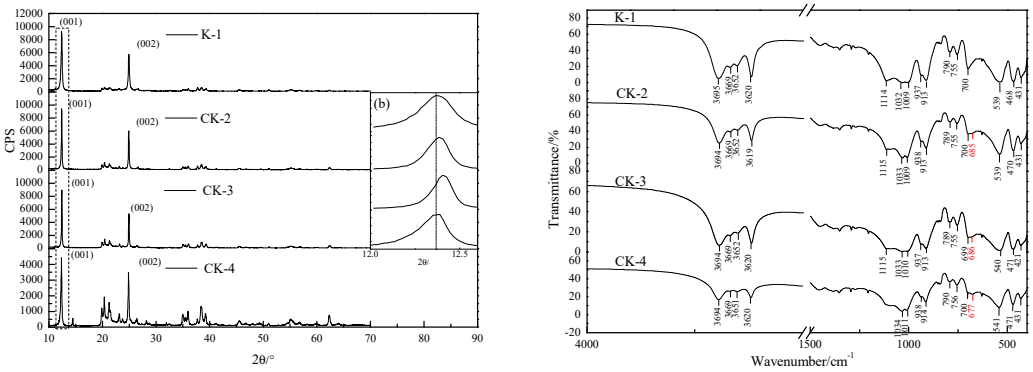

(**a**) (**b**)

Figure 3. XRD and FTIR spectra of all kaolinite samples. (**a**) XRD; (**b**) FTIR spectra.

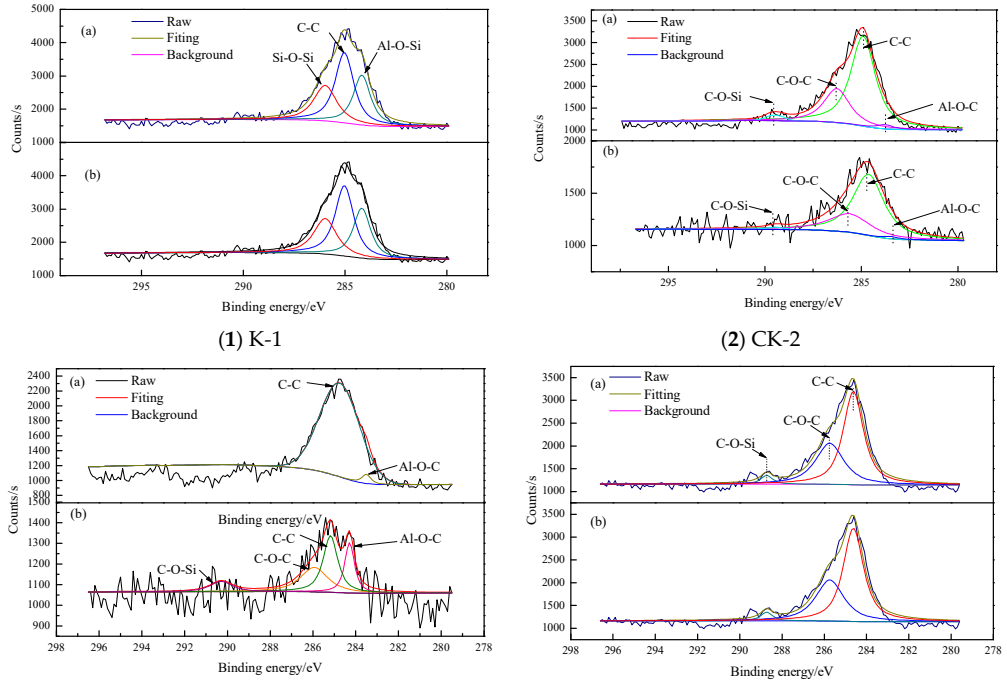

(**1**) K-1 (**2**) CK-2

(**3**) CK-3 (**4**) CK-4

Figure 4. The XPS Spectra of C 1s for non-coal kaolinite and coal kaolinite: (**a**) Before etching; (**b**) After etching.

3.1.3. FTIR

The FTIR diffuse reflection spectra of kaolinites can be divided into high frequency (3700–3600 cm^{-1}) and low frequency (1200–400 cm^{-1}). Farmer [30] thinks that there existed four characteristic adsorption peaks around 3695, 3670, 3651 and 3620 cm^{-1} in the pure kaolinite. For the four samples, the wavenumber of the FTIR spectra and their corresponding bonds are same. Among them, the bands around 3695, 3670, 3650 and 3620 cm^{-1} were found in Figure 3b, which were assigned to the inner-surface hydroxyls and the inner hydroxyl, respectively [31]. The adsorption peak around 1114 cm^{-1} was the symmetric stretching vibration and 1033 and 1010 cm^{-1} were the antisymmetric stretching vibrations of the Si-O-Si bond, as shown in Table 3. The adsorption peaks around 937 and 913 cm^{-1} were caused by the bending vibration of the inner-face and the inner hydroxyls, respectively. The translation vibration of hydroxyl was 790 cm^{-1}. The bands at about 755 and 697cm^{-1} were the stretching vibrations of the Si-O bond. Another peak band, located at 432 cm^{-1}, can be assigned to the bending vibration of the O-Al-O bond [32–35].

Table 3. FTIR vibrational frequencies (cm^{-1}) of non-coal kaolinite and coal kaolinite.

Reference Value/cm^{-1} [35,36]	Vibrational Frequencies/cm^{-1}				Proposed Assignment
	K-1	CK-2	CK-3	CK-4	
3695	3695	3694	3694	3694	OH stretching vibration
3670	3669	3669	3669	3669	OH stretching vibration
3651	3652	3652	3652	3651	OH stretching vibration
3621	3620	3619	3620	3620	OH stretching vibration
1114	1114	1115	1115	1114	Si-O-Si symmetric stretch
1034	1032	1033	1033	1034	Si-O-Si antisymmetric stretch
1012	1009	1009	1010	1011	Si-O-Si antisymmetric stretch
937	937	938	937	938	OH bending vibration
915	913	913	913	914	OH bending vibration
794	790	789	789	790	Si translation
755	755	755	755	756	Si-O stretching vibration
697	700	700	699	700	Si-O stretching vibration
685	685	685	686	677	Al-OH vertical vibration
540	539	539	540	541	O-Si-O bend + CO stretch
473	468	470	471	471	O-C-O bend + CO stretch
432	431	431	431	431	O-Al-O bend

Note: The numbers in each row are the vibrational frequencies. The content in the last column is the corresponding functional group.

Compared with the non-coal kaolinite, there existed some differences between the vibration bands of coal kaolinite. It was found that 539, 468 cm^{-1} gradually shifted to 541, 471 cm^{-1}, which may be attributed to the CO stretching and OCO bending vibration, instead of SiO stretching and OSiO bending vibration. Meanwhile, a small new band at about 686 cm^{-1} appeared, which implies that C atoms enter into the structure, replace the Si of kaolinite and affect the vibration–rotation energy of kaolinite.

3.1.4. XPS

In order to further study the existence of elements, such as Al, Si, O and C, X-ray photoelectron spectroscopy was conducted as an effective analysis technique. According to the position of the photoelectron absorption peak (electron binding energy), it can identify the elements in the sample and the different forms of the same elements in the compound. The binding energy of Si 2p, Al 2p and O 1s electrons and their existing bonds in all four samples were very close to one another. Before and after etching, the Si 2p spectra show strong peaks at 103.00–103.55 eV, which belong to the Si-O bond. The Al 2p spectra show strong peaks at 74.84–75.74 eV, indicating the Al-O bond. The O 1s spectrum shows strong peaks in the range of 531.9–532.33 eV, which could indicate the existence of Si-O, Al-O and Si-O-Si bonds. The above binding energies are consistent with the silicon and aluminum oxides [37,38].

As the K-1 and CK-3 samples are both powders, their XPS spectra of C 1s are same before and after etching, as is clearly shown in Figure 5. Before and after etching, the C 1s spectrum of coal kaolinite shows a strong peak around 284.60 eV, which belongs to the C-C bond of aromatic carbon on the kaolinite surface, covered with incomplete dissociated impurity coal. Meanwhile, the curve-fitting peaks around 283.50 and 288.90 eV appeared, which revealed that Al-O-C and C-O-Si bonds were formed instead of Al-O-Si and Si-O-Si bond. These results were attributed to the substitution of the carbon atom for silicon atoms in the kaolinite lattice in the process of coal formation, as is clearly shown in Figure 6. However, the contents of the latter two are relatively small.

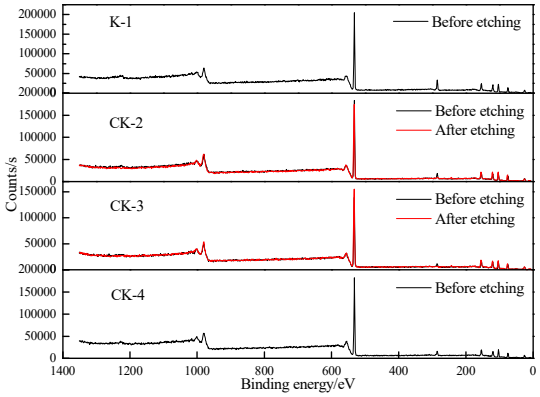

Figure 5. The XPS Spectrum of all samples.

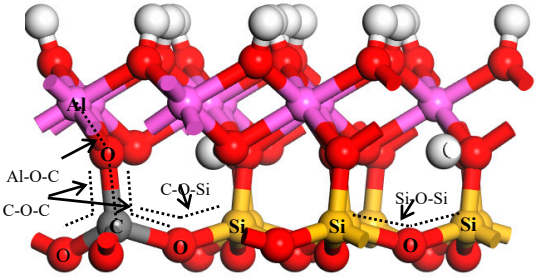

Figure 6. Surface model of coal kaolinite.

3.2. The Doping Mechanism and Impurity Substitution Energies

According to the isomorphism principle, the carbon atoms were most likely to substitute for the Si or O atoms of the kaolinite (001) surface, including the Si-O-(001) surface and Al-O-(001) surface, so that the substitution models, as shown in Figure 7b,c,e, represented the coal pyrite in the present study. For the coal kaolinite, the Si atom and O atom of both sides may be substituted. Therefore, the impurity substitution energies were calculated, as shown in Table 4.

Table 4. Impurity substitution energy of the pyrite surface substituted by carbon atoms.

Surface	The Substituted Atom	ΔE/kJ/mol
Si-O-(001)	Si	258.12
	O	660.01
Al-O-(001)	O	469.92

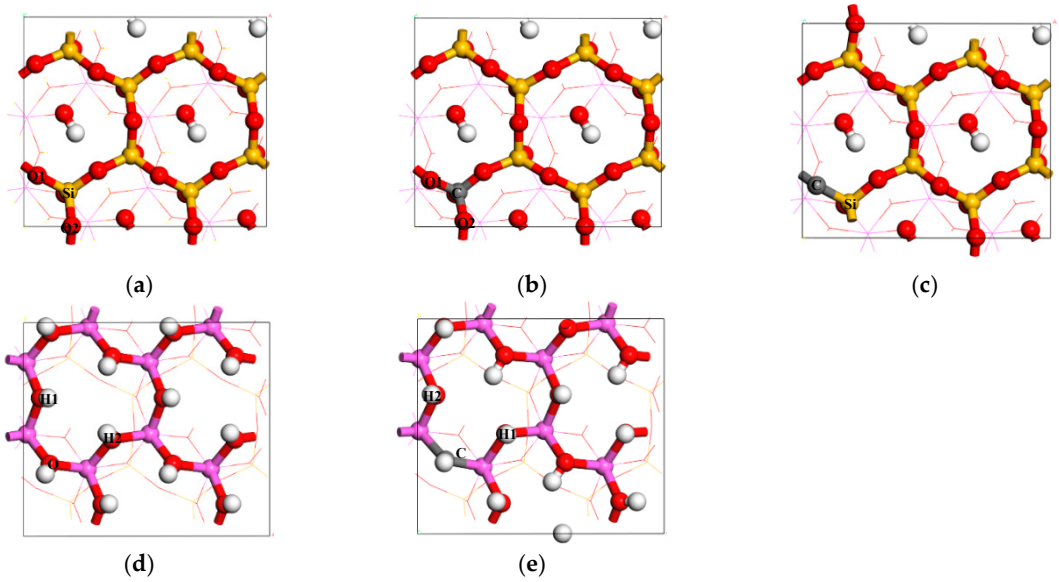

Figure 7. The one carbon atom-substituted configuration of the kaolinite (001) surface: (**a**) Si-O-(001)-undoped; (**b**) Si-O-(001)-doped (Si); (**c**) Si-O-(001)-doped (O); (**d**) Al-O-(001)-undoped; (**e**) Al-O-(001)-doped (O).

For the Si-O-(001)-doped (Si) and Si-O-(001)-doped (O), the ΔE were 258.12 kJ/mol and 660.01 kJ/mol, respectively. This demonstrated that, whether the carbon atom substituted the Si atom or O atom, it was not spontaneous and a large amount of external energy was needed to induce this chemical reaction. The former was easier to in the coal-forming process because of its smaller impurity substitution energy, which may be due to the fact that the C atom and the Si atom belong to the same main element group and their properties are close. For the Al-O-(001)-surface, the ΔE was 469.92 kJ/mol after the O atom was substituted by the C atom. In summary, a minimum energy was needed if the Si atom of Si-O-(001) surface was substituted by the C atom, and the carbon atom was the easiest to substitute for the silicon atom and the most difficult to substitute for the oxygen atom of the Si-O-(001) surface. So, the models of Si-O-(001)-doped (Si) were used as the surface models to study the effect of the carbon atom-defect on the structure of kaolinite.

3.3. Interplanar Spacing of Kaolinite

The XRD and XPS results showed that the interplanar spacing decreased due to the substitution of silicon atoms by carbon atoms. So, the double-layer model of the coal kaolinite (001) surface, doped with different amounts of carbon atoms, was further optimized and the interplanar spacing was calculated as follows:

$$d = \Delta Z = Z_U - Z_L \quad (4)$$

where d is the interplanar spacing, ΔZ is the Z coordinate difference of Aluminum atomic number. Z_U is the Z coordinate of the upper aluminum atom and is the Z_L coordinate of the lower aluminum atom.

The interplanar spacing of non-coal kaolinite is 7.15440, close to the experimental value of 7.1543, which explained that the selected model is scientific and reasonable. Compared with the non-coal kaolinite, the interplanar spacing of coal kaolinite becomes small after the Si atoms are substituted by the C atom and decreased gradually with the increase in the doping number of carbon atoms (7.15440 Å→7.11859 Å→7.10902 Å→7.10105 Å), as shown in Table 5. This shows that the crystal of coal kaolinite shrinks during to the substitution of carbon atoms for silicon atoms. It was found that, due to the long-term coal forming environment, the carbon atoms with smaller atomic radii (0.077nm) in the coal replace the silicon atoms with larger atomic radii (0.117nm) in the coal kaolinite, which leads

to the contraction of the crystal surfaces and the decrease in the interplanar spacing, which is consistent with the experimental results of XRD and XPS.

Table 5. Interplanar spacing of non-coal kaolinite and coal kaolinite.

Aluminum Atomic Number	Aluminum Atomic Coordinates	Non-Coal Kaolinite	Coal Kaolinite-1	Coal Kaolinite-2	Coal Kaolinite-3
1	Z_U/Å	−2.64081	−2.66453	−2.71756	−2.55374
	Z_L/Å	−9.78855	−9.77141	−9.77409	−9.70512
	ΔZ_1/Å	7.14774	7.10688	7.05653	7.15138
2	Z_U/Å	−2.63644	−2.69702	−2.75039	−2.64026
	Z_L/Å	−9.79749	−9.80136	−9.79238	−9.76588
	ΔZ_2/Å	7.16105	7.10434	7.04199	7.12562
3	Z_U/Å	−2.64081	−2.65630	−2.63457	−2.83543
	Z_L/Å	−9.78855	−9.78368	−9.78957	−9.78204
	ΔZ_3/Å	7.14774	7.12738	7.15500	6.94661
4	Z_U/Å	−2.63644	−2.63728	−2.60317	−2.59814
	Z_L/Å	−9.79749	−9.77303	−9.78574	−9.77874
	ΔZ_4/Å	7.16105	7.13575	7.18257	7.18060
ΔZ		7.15440	7.11859	7.10902	7.10105

Note: The Alminum atomic numbers 1, 2 3 are 4 are shown in Figure 8. The coal kaolinite-1 represents the kaolinite (001) surface doped by one carbon atom. The coal kaolinite-2 represents the kaolinite (001) surface doped by two carbon atoms. The coal kaolinite-3 represents the kaolinite (001) surface doped by three carbon atoms.

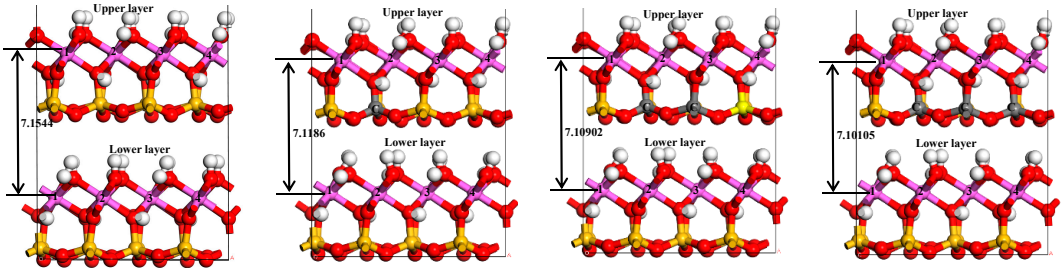

(**a**) Non-coal kaolinite (**b**) Coal kaolinite-1 (**c**) Coal kaolinite-2 (**d**) Coal kaolinite-3

Figure 8. Configurations of kaolinite (001) surface with different amounts of carbon atoms.

4. Conclusions

The mineralogical characteristics of between non-coal kaolinite and coal kaolinite were compared. The doping of the carbon atom appeared to incorporate into the kaolinite instead of the silicon atoms of the layered stacking coal kaolinite surface. The Al-O-C, C-O-Si and C-O-C bonds were formed instead of the Al-O-Si and Si-O-Si bonds, resulting in a reduction in the interplanar spacing and the contraction of the crystal surface. The calculated interplanar spacing of coal kaolinite decreased with the increase in doping carbon atoms, which agreed well with the experiment. It provided an important theory for subsequent research on the properties of non-coal kaolinite and coal kaolinite and their further processing and utilization.

Author Contributions: Conceptualization, P.X.; methodology, P.X.; software, W.L.; validation, P.X.; formal analysis, P.X.; investigation, P.X.; resources, P.X.; data curation, P.X.; writing—original draft preparation, P.X.; writing—review and editing, P.X.; visualization, P.X.; supervision, R.M.; project administration, P.X.; funding acquisition, P.X. All authors have read and agreed to the published version of the manuscript.

Funding: This research was funded by the Fundamental Research Funds for the Central Universities (Grant No. 3142017102), Scientific Research Project in Colleges and Universities in Hebei Province (Grant No. QN2020506), a Project Funded by National Natural Science Foundation of China (Grant No. 51674137) and Nature Science Foundation of Hebei Province (E2019508097, E2020508029 and E2018508105). The APC was funded by the Fundamental Research Funds for the Central Universities (Grant No. 3142017102).

Acknowledgments: We thank Y. Han for providing the optimized single-layer model of the kaolinite (001) surface, the most stable adsorption model of water molecules on the kaolinite (001) surface, and T. Ma, J. Chen and Q. Yang for providing the coal kaolinite sample.

Conflicts of Interest: The authors declare no conflict of interest.

Abbreviation

All nomenclature and abbreviations were explained in alphabetical order, as follows:

BFGS:	Broyden–Fletcher–Goldfarb–Shanno;
CASTEP:	Cambridge Sequential Total Energy Package;
DFT:	Density Functional Theory;
DFT-D correction:	Density Functional Theory Dispersion correction;
FTIR:	Fourier Transform Infrared Spectroscopy;
GGA-PBE:	Generalized Gradient Approximation—Perdew–Burke–Ernzerhof;
GGA-RPBE:	Generalized Gradient Approximation—Revised Perdew–Burke–Ernzerhof;
GGA-PW91:	Generalized Gradient Approximation—Perdew Wang 91;
GGA-WC:	Generalized Gradient Approximation—Wu and Cohen;
GGA-PBESOL:	Generalized Gradient Approximation—Perdew et al., 2008;
HKL:	Crystal surface index, such as (001), (111); LDA-CA-PZ: Local Density Approximation—Ceperley and Alder, 1980;
SEM:	Scanning Electron Microscopy;
XRD:	X-ray diffraction;
XPS:	X-ray Photoelectron Spectroscopy;
XRF:	X-ray Fluorescence Spectrometry.

The abbreviations of parameters that are involved in each equation were described afterwards.

References

1. Qi, X.; Kuang, Y.L. Effects of clay minerals on the surface properties of coal slime. *Coal Sci. Technol.* **2013**, *41*, 126–128.
2. Qi, X.; Kuang, Y.L. Clay Mineral Affected to Treatment of Coal Slurry Water. *Coal Eng.* **2013**, *2*, 102–105.
3. Han, Y.H. Quantum Chemistry Study on the Surface Properties and Dispersion of Kaolinite and Montmorillonite. Ph.D. Thesis, China University of Science and Technology, Beijing, China, 2017.
4. Yu, Y.X. The Study on Interparticle Interaction and the Effect on Coal Flotation. Ph.D. Thesis, China University of Science and Technology, Beijing, China, 2018.
5. Xi, P.; Liu, W.L.; Han, Y.H. Study on the mechanism of coal pyrite crystal lattice defects and floatability. *J. China Coal Soc.* **2016**, *41*, 997–1003.
6. Xi, P.; Liu, W.L.; Yang, Z.Y. Quantum chemistry investigation on influence of carbon atom adsorption in carbon material to the coal pyrite hydrophobicity. *J. China Coal Soc.* **2017**, *42*, 1290–1296.
7. Xi, P.; Ma, R.X.; Liu, W.L. Research on the effect of carbon defects on the hydrophilicity of coal pyrite surface from the insight of quantum chemistry. *Molecules* **2019**, *24*, 2285. [CrossRef]
8. Xi, P.; Shi, C.S.; Yan, P.K. DFT study on the influence of sulfur on the hydrophobicity of pyrite surfaces in the process of oxidation. *App. Sur. Sci.* **2019**, *466*, 964–969. [CrossRef]
9. Boussemghoune, M.; Chikhi, M.; Ozay, Y.; Guler, P. The investigation of organic binder effect on morphological structure of ceramic membrane support. *Symmetry* **2020**, *12*, 770. [CrossRef]
10. Hong, H.L.; Tie, L.Y.; Min, X.M. Surface chemistry of kaolinite by quantum chemistry calculations. *J. Wuhan Univ. Technol.* **2005**, *27*, 25–29.
11. Zhang, C.; Song, K.H.; Wang, X. Quantum chemical study of intercalation of water molecules in kaolinite. *J. Mol. Sci.* **2013**, *29*, 134–141.
12. Han, Y.H.; Liu, W.L.; Chen, J.H. DFT simulation of the adsorption of sodium silicate species on kaolinite surfaces. *App. Surf. Sci.* **2016**, *370*, 403–409. [CrossRef]
13. Tunega, D.; Bucko, T.; Zaoui, A. Assessment of ten DFT methods in predicting structure of sheet silicates: Importance of dispersion corrections. *J. Chem. Phys.* **2012**, *137*, 1–9. [CrossRef] [PubMed]

14. Zhang, G.F.; Feng, Q.M.; Lu, Y.P. Relation between crystallography properties and surface characteristics of kaolinite and its floatability. *Nonferrous Met.* **2001**, *2*, 22–25.
15. Han, Y.H.; Liu, W.L.; Zhou, J. Interactions between kaolinite Al-OH surface and sodium hexametaphosphate. *App. Surf. Sci.* **2016**, *387*, 759–765. [CrossRef]
16. Han, Y.H.; Liu, W.L.; Chen, J.H. Adsorption mechanism of hydroxyl calcium on two kaolinite (001) surface. *J. China Coal Soc.* **2016**, *41*, 743–750.
17. Segall, M.D.; Lindan, P.J.D.; Probert, M.J. First-principles simulation: Ideas, illustrations and the CASTEP code. *J. Phys. Condens. Matter* **2002**, *14*, 2717–2744. [CrossRef]
18. Vanderbilt, D. Soft self-consistent pseudopotentials in a generalized eigenvalue formalism. *Phys. Rev. B.* **1990**, *4*, 7892–7895. [CrossRef]
19. Tkatchenko, A.; Scheffler, M. Accurate Molecular Van Der Waals Interactions from Ground-State Electron Density and Free-Atom Reference Data. *Phys. Rev. Lett.* **2009**, *102*, 1–4. [CrossRef]
20. Pfrommer, B.; Côté, M.; Louie, S.; Cohen, M. Relaxation of crystals with the quasi-Newton method. *J. Comput. Phys.* **1997**, *131*, 233–240. [CrossRef]
21. Wang, X.Y.; Huang, Y.J.; Pan, Z.G.; Wang, Y.X.; Liu, C.Q. Theoretical investigation of lead vapor adsorption on kaolinite surfaces with DFT calculation. *J. Hazard Matter* **2015**, *295*, 43–54. [CrossRef]
22. Hu, P.W. Basic Research on Kaolinite based Conductive Mineral Materials. Ph.D. Thesis, Central South University, Changsha, China, 2012.
23. Chen, W.X. Clay-Stone of Kaolinite in the Perma-Carboniferous of Wester Shandong: Characteristics, Occurrence of Fe and Ti. Master's Thesis, Shandong University of Science and Technology, Qingdao, China, 2004.
24. Tian, Y.X.; Huang, S.P.; Wang, W.C. Molecular dynamics simulation of the intercalation of kaolinite with urea and water. *J.B. Univ. Chem. Technol.* **2007**, *34*, 599–603.
25. Cheng, H.F. Study on Intercalation and Exfoliation of Kaolinite and its Application in the Rubber Composite. Ph.D. Thesis, China University of Science and Technology, Beijing, China, 2011.
26. He, Q. Study of gold-bearing electronic structure and flotation behavior. Master's Thesis, Guangxi University, Nanning, China, 2015.
27. Liu, P. *Crystal Point Defect*; Science Press: Beijing, China, 2010.
28. Farmer, V.C. Differing effects of particle size and shape in the infrared and Roman spectra of kaolinite. *Clay Min.* **1998**, *33*, 601–604. [CrossRef]
29. Frost, R.L.; Locos, O.B.; Kristóf, J.; Kloprogge, J.T. Infrared spectroscopic study of potassium and cesium acetate-intercalated kaolinite. *Vin. Spectrosc.* **2001**, *26*, 33–42. [CrossRef]
30. Frost, R.L. Combination bands in the infrared spectroscopy of kaolinites-A drift spectroscopic study. *Clays Clay Min.* **1998**, *46*, 466–477. [CrossRef]
31. Yang, Z.Q.; Zhao, X.Y.; Zhang, L. Infra-red spectra analysis for clay minerals of kaolinite. *Exp. Pet. Geol.* **1988**, *10*, 60–66.
32. Wang, Y.G. Study on the degree of crystallinity of kaolinite in gangue. *Shanxi Chem. Ind.* **2014**, *151*, 19–22.
33. Xu, N.C.; Shen, J.L.; Luo, H.Y. Analysis for crystallinity of kaolinites by X-ray diffractometer and infrared spectroscopy. *Resour. Surv. Env.* **2014**, *35*, 153–156.
34. Daniel, B.; Konstantin, S.S.; Ekkehard, G. Vibrational spectra and structure of kaolinite: A computer simulation study. *J. Phys. Chem. B.* **2000**, *104*, 9210–9217.
35. Zhu, B.L.; Qi, C.L.; Zhang, Y.H.; Bisson, T.; Xu, Z.H.; Fan, Y.J.; Sun, Z.X. Synthesis, characterization and acid-base properties of kaolinite and metal (Fe, Mn, Co) doped kaolinite. *Appl. Clay Sci.* **2019**, *179*, 105–138. [CrossRef]
36. Moulder, J.F.; Stickle, W.F.; Sobol, P.E.; Bomben, K.D. *Handbook of X-Ray Photo-Electron Spectroscopy*; Physical Electronics Inc.: Chanhassen, MN, USA, 1995.
37. Rumble, J.R., Jr.; Bickham, D.M.; Powell, C.J. The NIST X-ray Photoelectron Spectroscopy Database. *Surf. Interface Anal.* **1992**, *19*, 241–246. [CrossRef]
38. Qin, S.; Wang, C.Q. *Basis of Mineralogy*; Peking University Press: Beijing, China, 2006.